CLIMATOLOGY

Synchronous crop failures and climate-forced production variability

W. B. Anderson[1,2,3]*, R. Seager[1], W. Baethgen[2], M. Cane[1], L. You[4,5]

Large-scale modes of climate variability can force widespread crop yield anomalies and are therefore often presented as a risk to food security. We quantify how modes of climate variability contribute to crop production variance. We find that the El Niño Southern Oscillation (ENSO), the Indian Ocean Dipole (IOD), tropical Atlantic variability (TAV), and the North Atlantic Oscillation (NAO) together account for 18, 7, and 6% of globally aggregated maize, soybean, and wheat production variability, respectively. The lower fractions of global-scale soybean and wheat production variability result from substantial but offsetting climate-forced production anomalies. All climate modes are important in at least one region studied. In 1983, ENSO, the only mode capable of forcing globally synchronous crop failures, was responsible for the largest synchronous crop failure in the modern historical record. Our results provide the basis for monitoring, and potentially predicting, simultaneous crop failures.

INTRODUCTION

Rapid increases in agricultural trade have notably changed the character of the global food production system in recent decades. The fraction of food produced for human consumption that is traded internationally rose from 15% in 1986 to 23% in 2009 (*1*). While fewer people than ever before have inadequate access to a sufficient quantity of food, an increasing number of people are dependent on imported food to meet daily minimum caloric needs (*2*).

A stated goal of agricultural trade liberalization is to stabilize commodity markets by making supply more resilient without requiring costly reserves of perishable grain (*3*). Poor harvests in one region may be compensated for by bumper harvests elsewhere if production failures are independent events, but global climate modes, such as the El Niño Southern Oscillation (ENSO), violate this tenet by forcing global-scale climate (*4*) and crop yield (*5*, *6*) anomalies. How important these global-scale risks are to modern-day food production is an open question.

Despite progress in understanding average yield anomalies (*7*) and the areal extent of yield anomalies (*6*) forced by climate modes, the relative importance of climate modes compared to other factors, such as weather (*8*) and pests (*9*), is poorly understood. Of particular interest to global food security is the potential for global climate modes to force globally synchronous crop failures (*10*), by which we mean the failure of a single crop in multiple regions simultaneously. In the absence of substantial changes to our food production system, these failures are projected to become increasingly frequent because of climate change (*11*).

Here, we quantify the relative contribution of major climate modes to the crop production variability of individual regions and to global production variance with particular attention to globally synchronous crop failures. Our results provide the basis for monitoring, and potentially predicting, simultaneous crop failures.

[1]Lamont-Doherty Earth Observatory, Columbia University, Palisades, NY, USA. [2]International Research Institute for Climate and Society, Palisades, NY, USA. [3]Department of Earth and Environmental Sciences, Columbia University, Palisades, NY, USA. [4]International Food Policy Research Institute, Washington, DC, USA. [5]Macro Agriculture Research Institute and College of Economics and Management, Huazhong Agricultural University, Wuhan, Hubei, China.
*Corresponding author. Email: weston@iri.columbia.edu

RESULTS

Climate modes

To identify how climate modes influence global crop yields, we perform a maximum covariance analysis (MCA) of the coupled modes of variability between climate and crop yields (see Materials and Methods). The first two global modes correspond to an ENSO life cycle (fig. S1); the first (second) time expansion coefficient of the sea surface temperature (SST) mode is significantly correlated with September, October, and November [March, April, and May (MAM)] Niño 3.4 index at $r = -0.98$ ($r = 0.90$). Regional analyses for the North Atlantic, Indian Ocean, and tropical Atlantic reveal climate modes that are significantly correlated with the December, January, and February (DJF) station-based North Atlantic Oscillation (NAO) index, July, August, and September (JAS) Indian Ocean Dipole (IOD) mode index, April, May, and June (AMJ) tropical South Atlantic index, and AMJ tropical North Atlantic index ($r = 0.89$, -0.7, -0.75, and 0.81, respectively). The patterns of climate variability resulting from a partial regression using the climate time expansion coefficient (Figs. 1 and 2; A_k in Eq. 2) closely resemble the patterns obtained by creating positive minus negative phase composites for each variable (not shown), which confirms that the modes that we identify capture relevant large-scale climate teleconnections. To discuss the causal pathway between each climate mode and its crop yield teleconnections, we adopt a region-by-region approach.

Regional analyses

Crop yields in Northeast Brazil, southwest Mexico, and West Africa are influenced by climate modes centered in the Pacific Ocean (Fig. 1 and fig. S1) and Atlantic Ocean (Fig. 2 and fig. S2) basins that affect growing season (boreal spring to fall) moisture availability. In Northeast Brazil, southwest Mexico, and West Africa, ENSO accounts for 38, 20, and 15% of local maize production variance (see Eq. 4 in Materials and Methods), while internal variability of Atlantic SSTs account for 28 and 26% of the variance in Northeast Brazil and West Africa (Fig. 3). During the summer of a developing El Niño, the intertropical convergence zone (ITCZ) remains closer to the equator in the Eastern Pacific, which decreases the moisture convergence south of Mexico (Fig. 1) and inhibits southerly moisture surges that bring rain to south-central Mexico (*12*), leading to poor maize harvests (*13*). The opposite is true during a developing La Niña. A mature

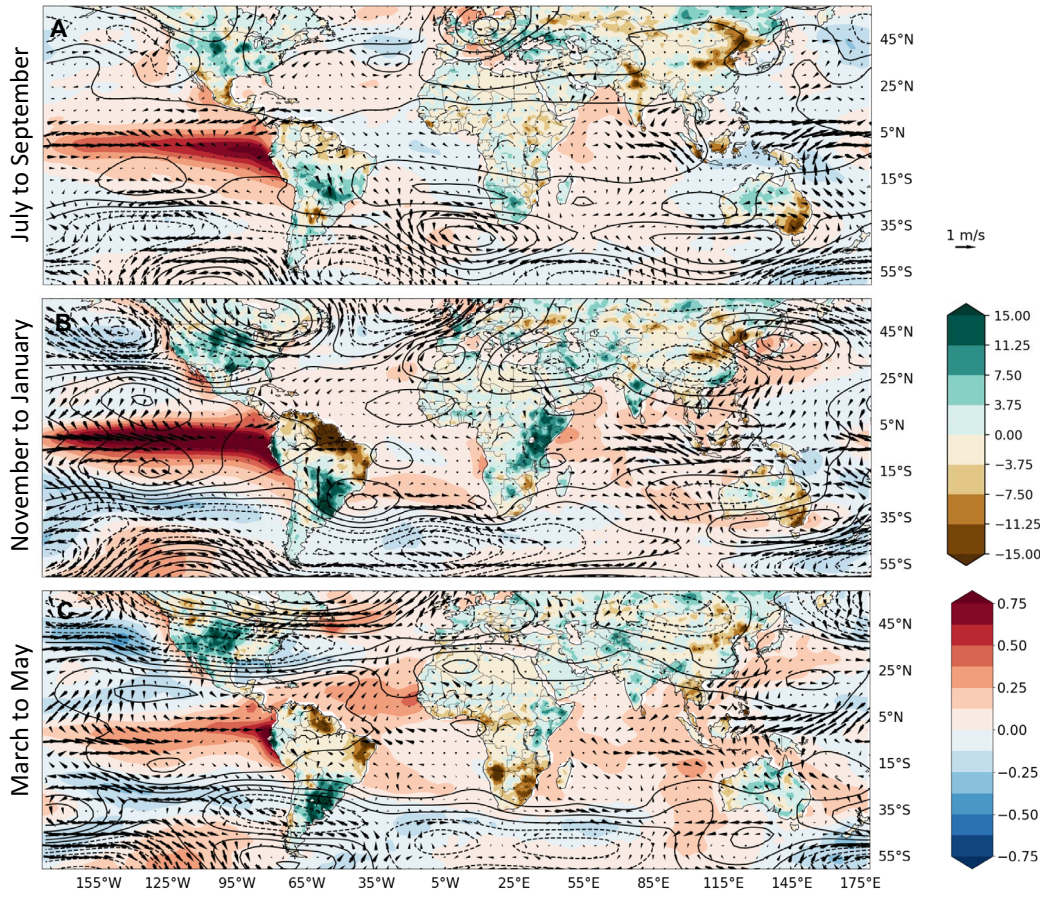

Fig. 1. El Niño climate teleconnections in JAS (July, August, September), NDJ (November, December, January), and MAM (March, April, May). Partial regression coefficients for the standardized ENSO time expansion coefficients 1 + 2 (A_1 * σ_{A_1} + A_2 * σ_{A_2} in Eq. 2) from the multilinear regression analysis. Partial regression coefficients are shown for three stages in the life cycle of an El Niño event: a developing El Niño (**A**), a mature El Niño (**B**), and a decaying El Niño (**C**). Colors are sea surface temperature anomalies (in °C) of the ocean and soil moisture anomalies (in kg/m^2) over land; contours are 200-hPa geopotential height anomalies (contours every 5 hPa), and vectors are winds at 925 hPa.

El Niño warms and stabilizes the troposphere throughout the tropics (Fig. 1) (*4*), which inhibits convection and thus favors drought in West Africa and Northeast Brazil (*4*, *14*). Furthermore, a mature El Niño warms SSTs in the north tropical Atlantic Ocean, which leads to a northward displacement of the ITCZ such that precipitation in Northeast Brazil is further inhibited (*14*). Internally generated tropical Atlantic variability (TAV) can enhance (or dampen) the positive meridional SST gradient, which amplifies growing season precipitation anomalies in northern Northeast Brazil (*14*) and West Africa (Fig. 2).

In southeast South America and the United States, climate variability explains 10 to 23% of crop production variability. Both regions are affected by Rossby wave trains forced by heating in the tropical Pacific (Fig. 1). During austral summer, a mature El Niño forces an anticyclonic (cyclonic) circulation anomaly to the east (west) of southeast South America that advects moisture into the region (*15*), which leads to above-median precipitation (*15*) and above-normal yields of maize and soybeans (fig. S1) (*16*). For wheat in southeast South America, however, additional precipitation during El Niños leads to an increased probability of disease and increased cloudiness that decreases insolation (*17*), both of which lower yields. In the Northern Hemisphere, a mature El Niño (La Niña) excites a Rossby wave response (*4*) that leads to increased (decreased) wintertime precipitation in the southern United States, which persists through the following spring as soil moisture anomalies (Fig. 1) to positively (negatively) influence wheat yields (fig. S1) in the southern Great Plains (*18*, *19*). A developing El Niño (La Niña) affects maize (*20*) and soybean yields by forcing a trough (ridge) over the Midwest that leads to decreased (increased) heat and drought (*18*), although the dynamics are not well understood.

Australian and East African crop yields are affected by both the IOD and ENSO (Figs. 1 and 2 and figs. S1 and S2). Together, the two modes contribute to 30 to 41% of wheat production variability (Fig. 3). During the Ethiopian Kiremt (JAS) growing season, developing El Niños stabilize the tropical troposphere, which reduces precipitation over Ethiopia (Fig. 1) (*21*), causing crop failures. The El Niño of 2015/2016 is a compelling example (*22*). Six months later, during austral summer, however, El Niños warm Indian Ocean SSTs and force a precipitation dipole in Eastern Africa such that Southeastern Africa is drier than normal but the Horn of Africa "short rains" season is wetter than normal (Fig. 1). A mature El Niño warms SSTs and leads to increased convective heating in the western Indian Ocean, which forces a low-level cyclonic circulation off the southeast coast of Africa and decreases moisture flux convergence into Southeastern Africa (*23*), leading to drier than normal conditions and crop failures (*22*). In southeast Australia, La Niñas and negative IOD states

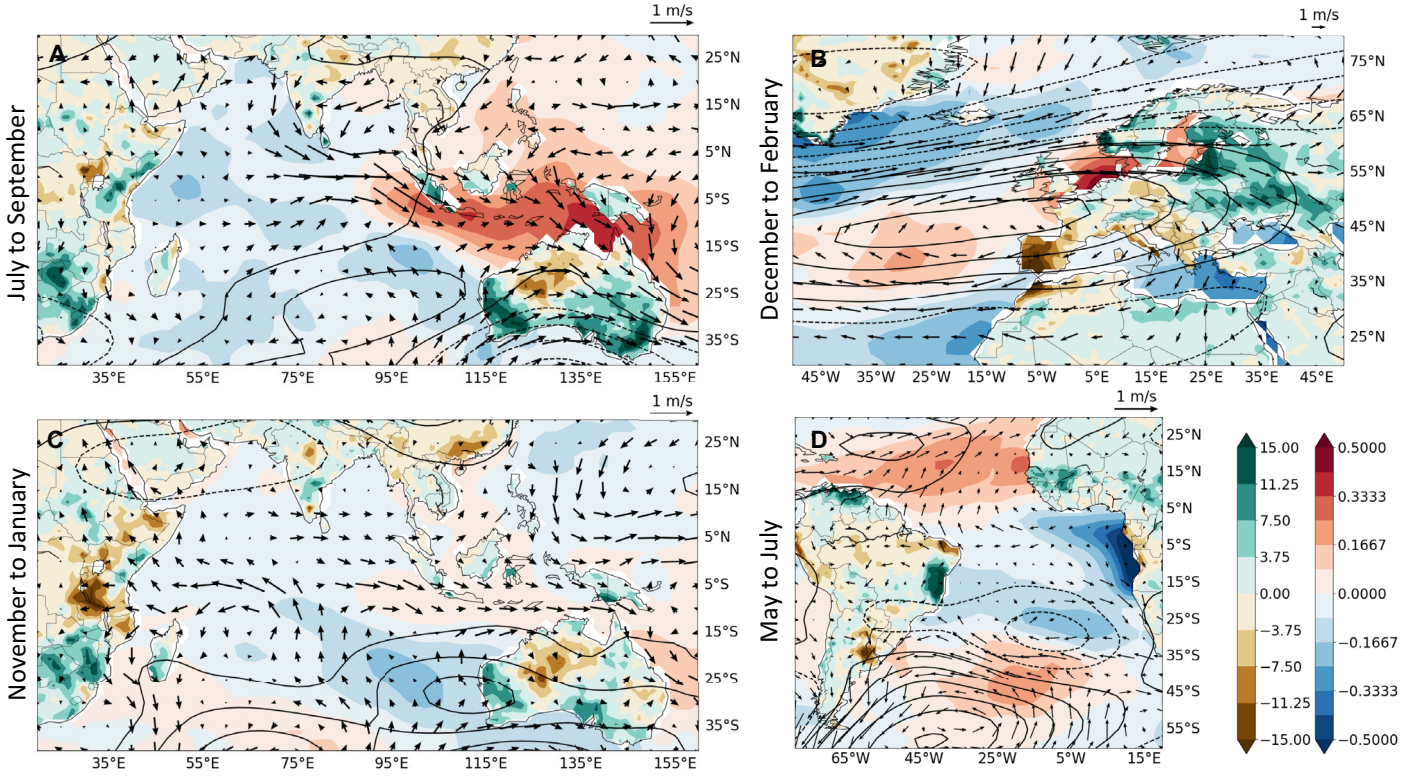

Fig. 2. Climate teleconnections for the Indian Ocean Dipole (IOD), Tropical Atlantic Variability (TAV), and North Atlantic Oscillation (NAO). Partial regression coefficients for the standardized IOD, TAV, or NAO time expansion coefficients ($A_k * \sigma_{A_k}$ in Eq. 2) on dependent climate variables. IOD coefficients during JAS (**A**) and NDJ (**C**). The NAO coefficients for DJF (B) and TAV coefficients during May, June, and July (**D**). Colors are SST anomalies of the ocean (in °C) and soil moisture anomalies over land (in kg/m^2). Contours are 200-hPa geopotential height anomalies (contours every 5 hPa for TAV and IOD and every 15 hPa for NAO), and vectors are winds at 925 hPa.

lead to increased precipitation (Figs. 1 and 2) (*24*) and positive winter wheat yields (fig. S2) (*25*), while El Niños and positive IOD states favor droughts and poor wheat yields (*24*, *25*) by forcing an anticyclonic circulation and descent that extends over much of Australia (Fig. 2).

In China and India, ENSO accounts for 26 and 25% of maize production variability but has a much smaller influence on wheat production because of extensive irrigation of wheat (*26*). Crops grown in India are divided into Kharif crops (e.g., maize) grown during the summer monsoon from June to September and Rabi crops (e.g., winter wheat) planted after the summer monsoon. During an El Niño, decreased summer monsoon precipitation (Fig. 1) damages Kharif crop yields (fig. S1) and leads to depleted soil moisture during the early weeks of the Rabi season, which depresses yields in the following harvest (*27*). In the North China Plain, a developing La Niña (El Niño) leads to above (below) expected maize yields (fig. S1) (*28*). One hypothesis for this teleconnection is that increased convection in the western North Pacific during a developing El Niño shifts the subtropical high southward and weakens it during midsummer, bringing precipitation to the Yangtze River valley but drought further to the north (Fig. 1) (*29*).

In both Europe (*30*) and North Africa (*31*), the NAO has a strong influence on wintertime climate. Climate variability accounts for ~14% of winter wheat production variance in Europe but ~64% in North Africa (Fig. 3). The disparate strength of influence between North Africa and Europe is likely related to the forms of abiotic stress imposed by the NAO in each region. In North Africa and Spain, wheat is primarily moisture limited and the NAO affects wheat yields by altering moisture availability, while in central Europe and Scandinavia, the temperature teleconnection is stronger (*32*). A positive NAO leads to reduced precipitation (*31*) and soil moisture in North Africa (Fig. 2), which leads to poor wheat yields (fig. S2). In parts of Scandinavia, the Balkans, and central Europe, positive NAOs produce relatively mild winters (Fig. 2) that reduce frost kill risks to winter wheat and lead to above expected yields (fig. S2). In Europe, both ENSO and the NAO affect winter wheat yields (Fig. 3), but ENSO does so by forcing NAO-like atmospheric states in the North Atlantic (*33*).

Global analysis

When considering all growing regions, climate modes account for 23, 17, and 15% of local maize, wheat, and soybean production variability (Fig. 4, A, C, and E; see Eq. 4 in Materials and Methods). According to past estimates (*8*), climate-related stresses (i.e., both weather- and climate mode–related) account for 32 to 39% of global wheat, soybean, and maize yield variability. Climate modes and weather, therefore, contribute roughly equally (~15 to 20%) to the overall climate-related crop yield variance.

In Fig. 4 (B, D, and F), we separate the production statistics into quartiles of production intensity to demonstrate that the total local variance in Fig. 4 (A, C, and E) largely reflects the variance in high-production regions. However, climate modes have a substantial effect on production variance in low-production regions as well, and teleconnections to maize remain comparable to or stronger than teleconnections to wheat and soybean in all quartiles. The influence of the NAO on wheat production variance at the global scale, however, reflects its influence in high-production systems, while

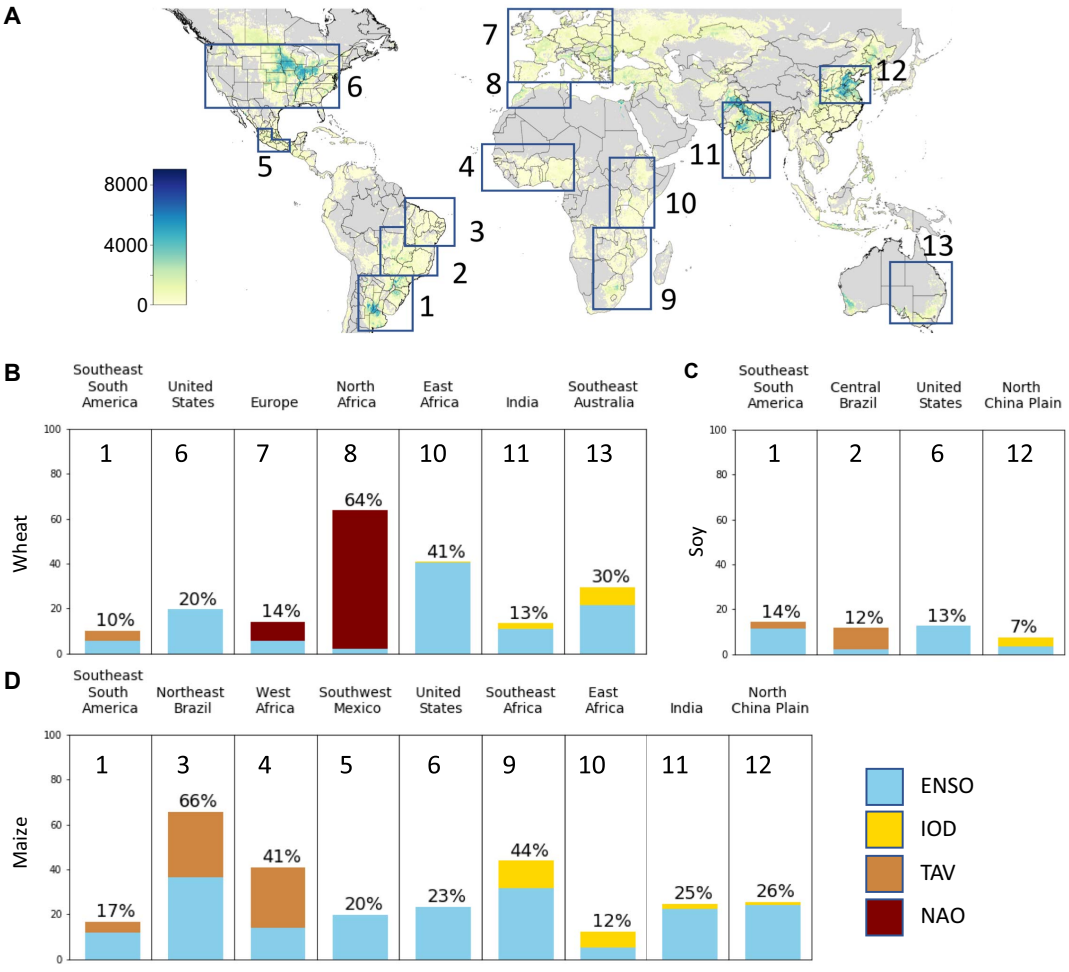

Fig. 3. Local production variance associated with climate modes. Harvested area of wheat, maize, and soybean with numbered boxes indicating regions for the variance analysis (**A**). Percent of national or subnational scale variance in each region for wheat (**B**), soybean (**C**), and maize (**D**) explained by the ENSO (El Nino Southern Oscillation), IOD, TAV, or NAO. The percent values on top of each bar indicate the total variance explained by modes of climate variability (ENSO + TAV + IOD + NAO).

the TAV's influence on maize variance at a global scale is muted because it primarily affects low-production regions. ENSO consistently contributes to the variance of both high- and low-production systems for all crops.

The tendency for maize to be more strongly affected by climate modes than wheat or soybeans holds true at both the regional (Fig. 3) and global (Fig. 4) scale. The heavy irrigation of wheat in China and India (*34*) explains the muted effect of climate modes on wheat. However, neither soybeans nor maize tends to be irrigated (*34*), and even in areas where they are cultivated during similar seasons, maize is more strongly affected by climate modes (Fig. 3). The discrepancy between maize and soybeans may be due to the relatively higher water demand of maize and soybeans are an indeterminate crop, one having a distribution of flowering dates rather than a single flowering date. Both of these characteristics make soybeans less sensitive than maize to a precipitation deficit during the growing season.

Climate modes account for 18% of variability of global maize production but only 7 and 6% of variability of global soybean and wheat production (Fig. 4, A, C, and E). The difference between the globally aggregated and local variance indicates that positive and negative climate teleconnections to maize yields are only minimally offsetting, while teleconnections to wheat and soybean yields are substantially offsetting.

The degree to which a climate mode forces offsetting crop yield anomalies depends on how the spatial distribution and intensity of climate teleconnections intersect the distribution and intensity of crop production. The compensating yield anomalies produced by the NAO are straightforward because they occur in a single region and season: A dipole in climate teleconnections (Fig. 2) leads to a dipole in yield anomalies (fig. S2) that substantially offsets one another. The degree to which ENSO leads to offsetting yield anomalies in a calendar year, however, is determined by how multiyear life cycles of ENSO teleconnections affect local crop growing seasons. Past research has demonstrated how life cycles of ENSO teleconnections can lead to offsetting growing conditions in major wheat, maize, and soybean producing regions (*34*), but these analyses do not describe the extent to which compensating environmental conditions translate into offsetting production anomalies. In the following section, we discuss ENSO teleconnections in terms of crop production anomalies and the degree to which they do or do not offset one another to dampen global-scale production variability.

Offsetting ENSO teleconnections

ENSO events develop in boreal summer, peak in the winter, and decay the following spring, so any given calendar year will be either a developing,

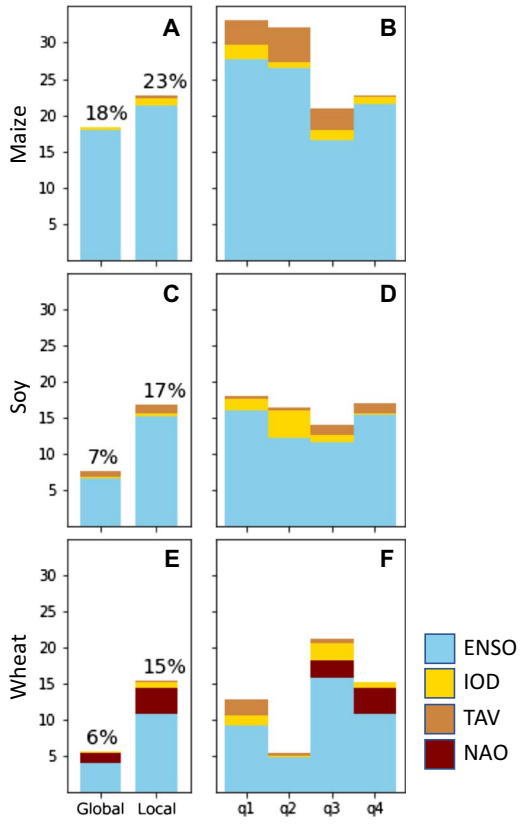

Fig. 4. Production variance associated with climate modes at the global scale and disaggregated by production quartile. Percent variance explained by each climate mode in the global domain when production variance is measured at the national or subnational scale ("local") or measured in the globally aggregated time series ("global") for maize (**A**), soybean (**C**), and wheat (**E**). See Materials and Methods for details. Percent of local variance explained disaggregated by average absolute production (in kg) quartile for maize (**B**), soybean (**D**), and wheat (**F**). Results ordered from lowest-production quartile (q1) to highest-production quartile (q4). Colors refer to variance related to the ENSO, IOD, TAV, or NAO.

decaying, or transitioning (e.g., El Niño to La Niña) ENSO event. For soybeans, ENSO forces moderate production anomalies in the United States during a developing year and in southeast South America during a decaying year, but these anomalies offset one another in a transition year (table S1 and fig. S1). For wheat, a developing ENSO event forces production anomalies in Eurasia that are partially offset by anomalies in the United States, while a decaying event produces same-sign anomalies in Australia and southeast South America. In a transitioning year, the wheat production anomalies offset one another (table S1). For maize, large production anomalies in the United States during a developing year are only partially offset by anomalies in India and China. During a decaying year, maize production anomalies in southeast South America are offset by those in Southeast Africa, West Africa, and Brazil.

Provided that soybean cultivation is more concentrated than that of maize, it may seem counterintuitive that ENSO teleconnections to soybeans are offsetting while teleconnections to maize are not, but this serves to highlight the importance of understanding how climate teleconnections intersect the distribution of cultivated lands. Soybean production is dominated by two regions: the United States (32% of production in 2010) and southeast South America (46% of production). During a transitioning ENSO year, ENSO-forced production anomalies in these regions effectively offset one another (table S1). ENSO teleconnections to maize yields are of the same sign as teleconnections to soybean yields (fig. S1), but the production anomalies are less effective at offsetting one another because of the relative distribution of maize production to the United States (31% of production) and southeast South America (8% of production). Maize production would be stabilized during ENSO years if production in the United States decreased and production in southeast South America, East Asia, and Southeast Asia increased. These changes would similarly decrease global production variance in non-ENSO years by moving maize production out of high-variance regions while maintaining global expected yields (*35*).

DISCUSSION

The global maize failures in 1983 were the most pronounced synchronous crop failure event in modern record (*10*). The 1983 El Niño was also one of the three strongest El Niños in at least the past 150 years. In Fig. 5, we plot the ENSO-forced yield anomalies as derived from our MCA analysis alongside the observed yield anomalies from 1983 to illustrate how large the influence of ENSO was on the synchronous crop failures of that year. The crop yield anomalies in 1983 are characteristic of an El Niño transitioning during the calendar year into a La Niña (compare Fig. 5 to fig. S1). The largest maize production failures occurred in southeast South Africa during the El Niño–forced drought in austral summer and in the United States during the following hot and dry boreal summer during La Niña. The observed and ENSO-forced patterns are notably similar, although the differing magnitudes of U.S. yield anomalies indicates that either nonlinear ENSO teleconnections or other factors were also at play. While 1983 is a case study, it is illustrative of the role that ENSO plays in forcing the most extreme synchronous maize failures.

Climate modes are, of course, only one of the many factors that affect crop yield variability. Crop yields are also affected by weather, pests, disease, and management decisions. While the relative importance of each factor will depend on the region in question, our results demonstrate that climate modes substantially affect crop yield variability on both regional and global scales.

ENSO, the IOD, TAV, and NAO are all important in at least one region studied, but only ENSO has a substantial influence on global production. Owing to the global scale of its influence and the distribution of maize production, ENSO has the potential to force globally synchronous maize failures, as it did in 1983. Historically, ENSO has not forced synchronous crop failures of wheat and soybean because of the distribution of cropland across regions with offsetting teleconnections or in regions that are weakly teleconnected, although this balance does not preclude large regional influences.

The trend toward a more interconnected global food system makes understanding the drivers of global-scale disruptions to food production necessary. Access to food and household welfare can be directly affected because of local crop failures, but it can also be indirectly affected by international trade, markets, and food prices (*36*). Our results indicate that climate modes can produce global-scale production anomalies, but further research is needed on how (and whether) these events translate to notable price shocks or export restrictions.

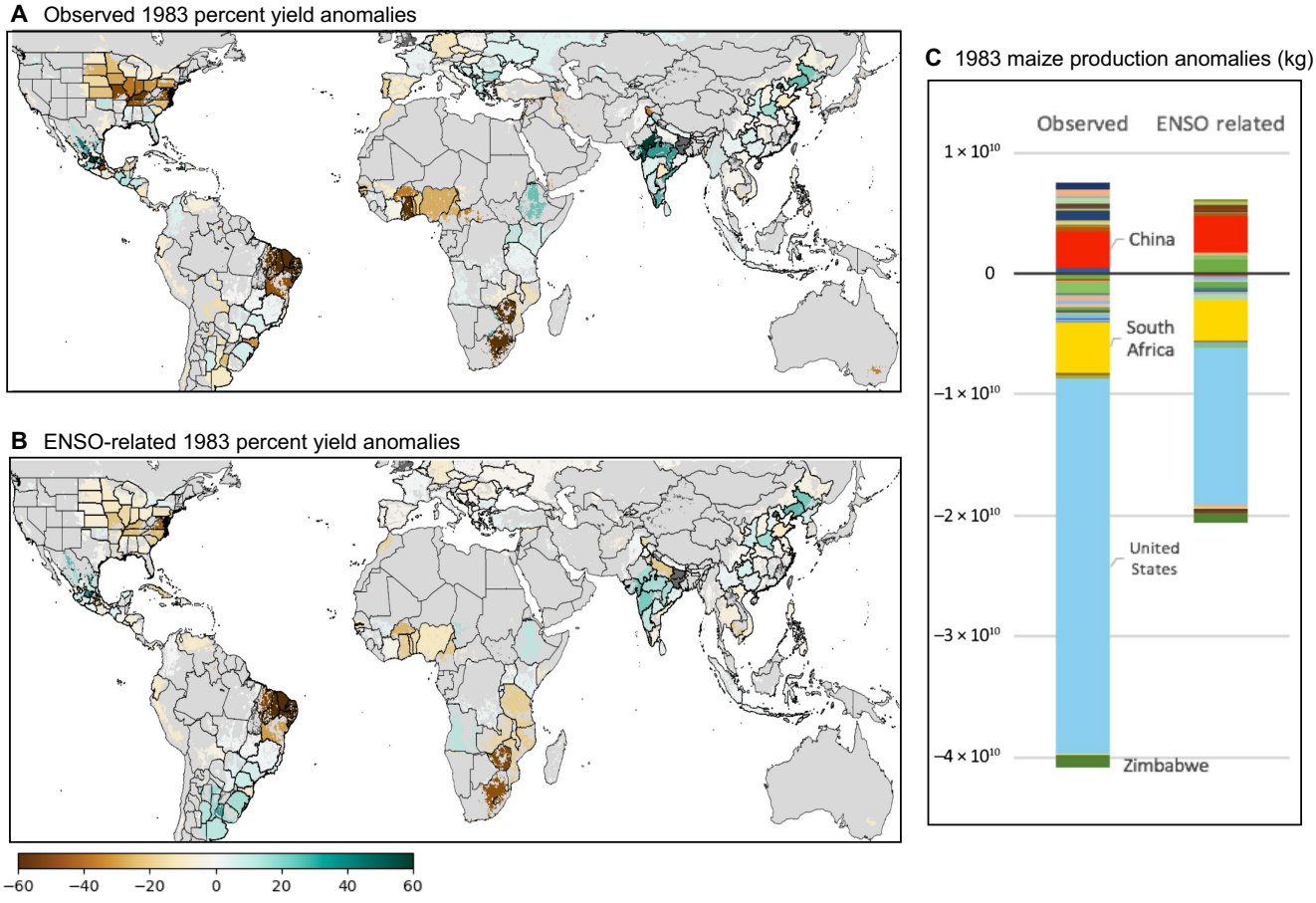

Fig. 5. Observed and ENSO-forced yield anomalies during the largest synchronous crop failure in modern historical record. Observed (**A**) and ENSO-forced (**B**) percent crop yield anomalies in 1983, which has been identified (*10*) as the most extensive synchronous crop failure in modern (after 1960) record, and maize production anomalies (**C**) by country. Both the spatial pattern and globally aggregated values indicate that ENSO played a major role in forcing synchronous crop failures in 1983. Observed crop yield anomalies are characteristic of an El Niño transitioning to a La Niña, as was the case in 1983 (compare to maize yield anomalies in fig. S1).

Table 1. Source of national and subnational crops statistics used in the analysis.

Country	Crop	Agency	Website
United States	Maize, wheat, and soybean	U.S. Department of Agriculture	http://quickstats.nass.usda.gov/
Argentina	Maize, wheat, and soybean	Integrated Agricultural Information System	www.siia.gov.ar/
Brazil	Maize, wheat, and soybean	Brazilian Companhia Nacional de Abastecimento	www.conab.gov.br/index.php
Canada	Wheat	Statistics Canada, CANSIM database	https://www150.statcan.gc.ca/t1/tbl1/en/cv.action?pid=3210035901#timeframe
India	Maize and wheat	Directorate of Economics and Statistics	https://eands.dacnet.nic.in/
Mexico	Maize	INEGI Information Databank	See Other Supplementary Materials (advances.sciencemag.org/cgi/content/full/5/7/eaaw1976/DC1): maize_yield_anoms.csv
China	Maize, wheat, and soybean	Ministry of Agriculture	http://zzys.agri.gov.cn/nongqing.aspx
Australia	Wheat	Australian Bureau of Statistics	www.abs.gov.au/
Other countries	Maize, wheat, and soybean	FAO	www.fao.org/faostat/en/

Recognizing the difference between random and structured risks to global agriculture creates an opportunity to plan for future global-scale disruptions to food production. Distinguishing ENSO- from weather-related droughts may seem semantic from the perspective of the maize plant, which fails in either case, but doing so is relevant to a country in West Africa that imports maize from Southeast Africa because both tend to experience drought and maize failures during an El Niño.

Our analysis provides the first global estimate of the degree to which modes of climate are responsible for crop production variability at regional and global scales. Independent of climate or crop models, our findings are an observationally derived estimate of the influence of climate modes on crop production variability.

MATERIALS AND METHODS

Subnational crop statistics from 1980 to 2010 were downloaded for crops in the United States, Argentina, Brazil, Canada, Mexico, India, China, and Australia (see Table 1). Food and Agriculture Organization (FAO) data were used where subnational data were unavailable. We used harvest year for all crops. We masked cropped areas on the basis of cells that have at least 0.01% harvested area for each crop (*37*).

For the climate analyses, we used SST anomalies from Extended Reconstructed SST v3b (*38*) and geopotential height and wind speed anomalies from the National Centers for Environmental Prediction–National Center for Atmospheric Research Reanalysis I (*39*). We standardized the SST field by multiplying each value by the square root of latitude and dividing by the standard deviation of the whole field. Over land, we used 0- to 1-m soil moisture from the Noah land surface model version 3.3 in the Global Land Data Assimilation System version 2 (*40*).

We calculated percent crop yield anomalies by first removing the long-term trend (the "expected yield") in each subnational unit using a low-frequency Gaussian filter with a kernel density of 3 years, which is similar to a 9-year running mean. Absolute yield anomalies were calculated as deviations from this long-term yield trend, which accounts for changes in management and technology at the subnational level. The absolute yield anomalies were divided by expected yield in each year to give the percent yield anomaly. Production anomalies, where used, were calculated as the product of the observed harvested area in each year and the absolute yield anomalies.

To isolate the influence of climate variability on crop yields, we used MCA (*41*). MCA uses a singular value decomposition (SVD) of the cross-covariance matrix between two fields—in this case, climate (SST or geopotential height) and percent crop yield anomalies (wheat, maize, and soy)—to identify the primary modes of covariance. By using MCA and focusing on covariance at a global scale, we attempted to separate yield anomalies forced by modes of climate variability from those forced by other factors. We expect that using MCA will separate localized weather-, pest-, or management-related crop failures from those that covary with climate modes. One benefit of using MCA to identify coupled modes of climate and crop yield covariance is that although it requires a choice of variables, there is no need to a priori choose a set of indices (of which there are many) to measure the activity of different climate modes.

To perform the MCA on SSTs and crop yield anomalies, we first construct the standardized $N \times M$ SST anomaly matrix, S, where N are all the observations from a calendar year ($N = 12$ months × number of locations) and M is the number of years. We similarly construct the standardized crop yield anomaly matrix, Y, by concatenating the wheat, maize, and soybean yield anomalies from a calendar year together to make a $K \times M$ matrix with K being observations for all crops in all countries and M being the number of years. The exception to this is the NAO, for which we restrict the influence of the winter NAO to a single crop, winter wheat. We then calculate the SVD of the cross-covariance matrix as

$$SY^T = U\Sigma V^T \quad (1)$$

where SY^T is the cross-covariance matrix. The orthonormal matrices U and V then contain the spatial SVD modes corresponding to the data fields S and Y, respectively, and Σ is a matrix with the singular values on the diagonal. The leading modes represent the primary patterns of covariance between the two fields. We next recover the time-expansion coefficients for each mode, k, as

$$A_k = U_k^T S; B_k = V_k^T Y \quad (2)$$

such that we can reconstruct the portion of the total variance in the data related to each SVD mode as

$$S_k = A_k U_k; Y_k = B_k V_k \quad (3)$$

The MCA analysis provides a series of spatial patterns (U and V) of climate and the associated crop yield anomalies forced by teleconnections from that climate mode. For example, when S is a matrix of tropical Pacific SSTs and Y contains crop yield anomalies of maize, soy, and wheat, the leading mode in U is a matrix of the monthly evolution of SST anomalies during an ENSO life cycle at each location in the tropics. The corresponding leading mode in V contains the covarying crop yield anomalies at each location, which are forced by teleconnections from ENSO. The time expansion coefficients for U and V represent how strongly each mode loads on each year and, in this example, would be closely related to indices measuring ENSO activity.

Agriculturally relevant teleconnections from most modes of variability occur primarily in a single season: The NAO in boreal winter affects precipitation in North Africa (*31*) and spring moisture availability in Europe (*30*); the TAV in spring affects rainy season precipitation in the Atlantic basin (*14*), and the IOD in late boreal summer affects Australian rainfall (*42*). For each mode of variability, therefore, we chose a domain that corresponds to the climate teleconnections from that mode during relevant growing seasons. ENSO, however, has global teleconnections that span the calendar year. For ENSO, therefore, we use global SSTs from 20°N to 20°S and global crop yields in the MCA analysis. After removing the influence of ENSO from the crop yield and SST fields by subtracting the ENSO-forced reconstruction (see Eq. 3), we repeated the MCA analysis for TAV and the IOD using the tropical Atlantic (20°N to 20°S, 60°W to 20°E) and Indian (20°N to 20°S, 35°W to 140°E) oceans with crop yields from countries in each basin (those shaded in Fig. 3). For the NAO, we used 500-hPa geopotential height anomalies in the domain 20°N to 80°N, 90°W to 40°E in conjunction with crop yields from Europe, the former Soviet Union, and the Mediterranean basin. For each mode of variability, we used climate variables from the season in which the mode was active: For ENSO, we used all months (January to December); for the IOD, we used July to September; for TAV, we used April to July; and for the

NAO, we used December to February. For each analysis, we used the first leading mode, or if the first two modes were not well separated from one another on the basis of their eigenvalues, we used the leading two modes. We explored whether leading modes of the MCA analysis related to other modes of climate variability, such as the Southern Annular Mode, the Scandinavian pattern, the East Atlantic index, or the Western Pacific index as well. The absence of leading modes that correspond to these indices in our analysis does not necessarily demonstrate that they are unimportant for crop yields but rather that any influence they may have is not separable, given the spatial resolution and length of available crop yield statistics.

We conducted a number of sensitivity analyses on the domains used for climate variables and the crop yield anomalies for the NAO, TAV, and IOD and found the results to be robust. We also tested an "ENSO-year" (May to April) for SST, which changes the partitioning of SST variance between modes 1 and 2 of the SVD but does not change the sum of the two modes or any of the results presented here.

After identifying the major coupled modes of variability, we confirmed that each mode corresponds to a known mode of climate variability using a series of linear multiple regression analyses, event composites, and correlations. In the linear multiple regression analysis, we computed regression coefficients between the time expansion coefficients as independent variables and either soil moisture, SST, geopotential height, or vector wind anomalies as the dependent variable. We then compared the results of the regression analysis with a series of positive minus negative event composites. For ENSO, for example, we compared the spatial pattern of regression coefficients obtained from the multiple regression analysis to an El Niño minus La Niña composite for the same climate variables. Last, we also compared the correlation between the time expansion coefficient of each mode and the corresponding climate index.

We calculated two types of production variance in this study: local variance and global variance. The local production variance measures the cumulative variance of all statistical reporting locations (i.e., states, provinces, countries, etc.) in a given domain. The global production variance measures the variance of a single global production anomaly time series and, by comparison to the local variance, provides a sense of whether the local production anomalies are additive (of the same sign) or offsetting (of opposite signs) when aggregated to a global scale. We calculate the local production variance as the sum of the squared vector norm of the absolute production anomaly time series

$$\|A\|^2 = \sum_{i,j} |\, a_{i,j} \,|^2 \qquad (4)$$

where A is a matrix that contains absolute production anomaly values $a_{i,j}$ for each location j and year i in a given domain. The global production variance is computed similarly, except that the vector norm is computed after summing the production values from all j locations into a time series of global production anomalies.

Our analysis relies on subnational and FAO country-level crop statistics, and while there are known issues with both (*43*, *44*), our methods minimize the degree to which poor data quality affects the results presented. Random errors in the crop yield data include those introduced by a reduced capacity of the FAO to accurately collect country-level data in Africa (*43*), while systematic errors include the over-reporting of achievements in Chinese statistics (*44*). Because both random and systematic errors are independent with respect to modes of climate variability, the MCA analysis is one means of separating the forced signal from this added noise or added bias. We do expect, however, that errors in the data degrade the strength of the relation between climate modes and crop yield anomalies in our analysis.

SUPPLEMENTARY MATERIALS

Supplementary material for this article is available at http://advances.sciencemag.org/cgi/content/full/5/7/eaaw1976/DC1

Fig. S1. SST and crop yield anomalies during a year transitioning from El Niño to La Niña.
Fig. S2. SST, geopotential height, and crop yield anomalies associated with the NAO, TAV, and IOD.
Table S1. Crop production anomalies during a year transitioning from El Niño to La Niña. Crop yield anomalies and long-term yield trends for each statistical reporting unit from 1980 to 2010.

REFERENCES AND NOTES

1. P. D'Odorico, J. A. Carr, F. Laio, L. Ridolfi, S. Vandoni, Feeding humanity through global food trade. *Earth's Future* **2**, 458–469 (2014).
2. M. Porkka, M. Kummu, S. Siebert, O. Varis, From food insufficiency towards trade dependency: A historical analysis of global food availability. *PLOS ONE* **8**, e82714 (2013).
3. D. G. Johnson, World agriculture, commodity policy, and price variability. *Am. J. Agric. Econ.* **57**, 823–828 (1975).
4. J. D. Horel, J. M. Wallace, Planetary-scale atmospheric phenomena associated with the Southern Oscillation. *Mon. Weather Rev.* **109**, 813 (1981).
5. M. Davis, *Late Victorian Holocausts: El Niño Famines and the Making of the Third World* (Verso Books, 2002).
6. M. Heino, M. J. Puma, P. J. Ward, D. Gerten, V. Heck, S. Siebert, M. Kummu, Two-thirds of global cropland area impacted by climate oscillations. *Nat. Commun.* **9**, 1257 (2018).
7. T. Iizumi, J.-J. Luo, A. J. Challinor, G. Sakurai, M. Yokozawa, H. Sakuma, M. E. Brown, T. Yamagata, Impacts of El Niño Southern Oscillation on the global yields of major crops. *Nat. Commun.* **5**, 3712 (2014).
8. D. K. Ray, J. S. Gerber, G. K. MacDonald, P. C. West, Climate variation explains a third of global crop yield variability. *Nat. Commun.* **6**, 5989 (2015).
9. E.-C. Oerke, Crop losses to pests. *J. Agric. Sci.* **144**, 31–43 (2006).
10. Z. Mehrabi, N. Ramankutty, Synchronized failure of global crop production. *Nat. Ecol. Evol.* **3**, 780–786 (2019).
11. M. Tigchelaar, D. S. Battisti, R. L. Naylor, D. K. Ray, Future warming increases probability of globally synchronized maize production shocks. *Proc. Natl. Acad. Sci. U.S.A.* **115**, 6644–6649 (2018).
12. V. O. Magaña, J. L. Vázquez, J. L. Pérez, J. B. Pérez, Impact of El Niño on precipitation in Mexico. *Geofís. Int.* **42**, 313–330 (2003).
13. M. Dilley, Climatic factors affecting annual maize yields in the valley of Oaxaca, Mexico. *Int. J. Climatol.* **17**, 1549–1557 (1997).
14. A. Giannini, R. Saravanan, P. Chang, The preconditioning role of tropical Atlantic variability in the development of the ENSO teleconnection: Implications for the prediction of Nordeste rainfall. *Clim. Dynam.* **22**, 839–855 (2004).
15. A. M. Grimm, V. R. Barros, M. E. Doyle, Climate variability in Southern South America associated with El Niño and La Niña events. *J. Climate* **13**, 35–58 (2000).
16. G. P. Podestá, C. D. Messina, M. O. Grondona, G. O. Magrin, Associations between grain crop yields in central-eastern Argentina and El Niño–Southern Oscillation. *J. Appl. Meteorol.* **38**, 1488–1498 (1999).
17. G. R. Cunha, G. A. Dalmago, V. Estefanel, in *Wheat in a Global Environment* (*Developments in Plant Breeding,* vol. 9), Z. Bedo, L. Lang, eds. (Springer, 2001), pp. 445–450.
18. W. Anderson, R. Seager, W. Baethgen, M. Cane, Life cycles of agriculturally relevant ENSO teleconnections in North and South America. *Int. J. Climatol.* **37**, 3297–3318 (2017).
19. S. A. Mauget, D. R. Upchurch, El Niño and La Niña related climate and agricultural impacts over the Great Plains and Midwest. *J. Prod. Agri.* **12**, 203–215 (1999).
20. P. Handler, Corn yields in the United States and sea surface temperature anomalies in the equatorial pacific ocean during the period 1868–1982. *Agric. For. Meteorol.* **31**, 25–32 (1984).
21. G. T. Diro, D. I. F. Grimes, E. Black, Teleconnections between Ethiopian summer rainfall and sea surface temperature: Part I—Observation and modelling. *Climate Dynam.* **37**, 103–119 (2011).
22. C. Funk, L. Harrison, S. Shukla, C. Pomposi, G. Galu, D. Korecha, G. Husak, T. Magadzire, F. Davenport, C. Hillbruner, G. Eilerts, B. Zaitchik, J. Verdin, Examining the role of unusually warm Indo-Pacific sea-surface temperatures in recent African droughts. *Q. J. R. Meteorol. Soc.* **144**, 360–383 (2018).
23. L. Goddard, N. E. Graham, Importance of the Indian Ocean for simulating rainfall anomalies over eastern and southern Africa. *J. Geophys. Res. Atmos.* **104**, 19099–19116 (1999).

24. C. C. Ummenhofer, M. H. England, P. C. McIntosh, G. A. Meyers, M. J. Pook, J. S. Risbey, A. Sen Gupta, A. S. Taschetto, What causes southeast Australia's worst droughts? *Geophys. Res. Lett.* **36**, L04706 (2009).
25. C. Yuan, T. Yamagata, Impacts of IOD, ENSO and ENSO Modoki on the Australian winter wheat yields in recent decades. *Sci. Rep.* **5**, 17252 (2015).
26. K. Krishna Kumar, K. Rupa Kumar, R. G. Ashrit, N. R. Deshpande, J. W. Hansen, Climate impacts on Indian agriculture. *Int. J. Climatol.* **24**, 1375–1393 (2004).
27. R. Selvaraju, Impact of El Niño–southern oscillation on Indian foodgrain production. *Int. J. Climatol.* **23**, 187–206 (2003).
28. Y. Liu, X. Yang, E. Wang, C. Xue, Climate and crop yields impacted by ENSO episodes on the North China Plain: 1956–2006. *Reg. Environ. Change* **14**, 49–59 (2014).
29. H. Ronghui, W. Yifang, The influence of ENSO on the summer climate change in China and its mechanism. *Adv. Atmos. Sci.* **6**, 21–32 (1989).
30. S. H. Baek, J. E. Smerdon, S. Coats, A. P. Williams, B. I. Cook, E. R. Cook, R. Seager, Precipitation, temperature, and teleconnection signals across the combined North American, Monsoon Asia, and Old World Drought Atlases. *J. Climate* **30**, 7141–7155 (2017).
31. P. J. Lamb, R. A. Peppler, North Atlantic Oscillation: Concept and an application. *Bull. Am. Meteorol. Soc.* **68**, 1218–1225 (1987).
32. P. Cantelaube, J.-M. Terres, F. J. Doblas-Reyes, Influence of climate variability on Europeanagriculture—Analysis of winter wheat production. *Climate Res.* **27**, 135–144 (2004).
33. A. A. Scaife, A. Arribas, E. Blockley, A. Brookshaw, R. T. Clark, N. Dunstone, R. Eade, D. Fereday, C. K. Folland, M. Gordon, L. Hermanson, J. R. Knight, D. J. Lea, C. MacLachlan, A. Maidens, M. Martin, A. K. Peterson, D. Smith, M. Vellinga, E. Wallace, J. Waters, A. Williams, Skillful long-range prediction of European and North American winters. *Geophys. Res. Lett.* **41**, 2514–2519 (2014).
34. W. Anderson, R. Seager, W. Baethgen, M. Cane, Trans-Pacific ENSO teleconnections pose a correlated risk to agriculture. *Agric. For. Meteorol.* **262**, 298–309 (2018).
35. T. Ben-Ari, D. Makowski, Analysis of the trade-off between high crop yield and low yield instability at the global scale. *Environ. Res. Lett.* **11**, 104005 (2016).
36. D. Headey, S. Fan, Anatomy of a crisis: The causes and consequences of surging food prices. *Agri. Econ.* **39**, 375–391 (2008).
37. F. T. Portmann, S. Siebert, P. Döll, MIRCA2000—Global monthly irrigated and rainfed crop areas around the year 2000: A new high-resolution data set for agricultural and hydrological modeling. *Global Biogeochem. Cycles* **24**, GB1011 (2010).
38. T. M. Smith, R. W. Reynolds, T. C. Peterson, J. Lawrimore, Improvements to NOAA's historical merged land–ocean surface temperature analysis (1880–2006). *J. Climate* **21**, 2283–2296 (2008).
39. E. Kalnay, M. Kanamitsu, R. Kistler, W. Collins, D. Deaven, L. Gandin, M. Iredell, S. Saha, G. White, J. Woollen, Y. Zhu, A. Leetmaa, B. Reynolds, M. Chelliah, W. Ebisuzaki, W. Higgins, J. Janowiak, K. C. Mo, C. Ropelewski, J. Wang, R. Jenne, D. Joseph, The NCEP/NCAR 40-year reanalysis project. *Bull. Am. Meteorol. Soc.* **77**, 437–472 (1996).
40. M. Rodell, H. Kato Beaudoing, "GLDAS Noah Land Surface Model L4 monthly 1.0 x 1.0 degree Version 2.0,version 020" (Technical Report NASA/GSFC/HSL (12.01.2013), Greenbelt, MA: Goddard Earth Sciences Data and Information Services Center, 2015); 10.5067/QN80TO7ZHFJZ.
41. C. S. Bretherton, C. Smith, J. M. Wallace, An intercomparison of methods for finding coupled patterns in climate data. *J. Climate* **5**, 541–560 (1992).
42. F. A. Schott, S.-P. Xie, J. P. McCreary Jr., Indian Ocean circulation and climate variability. *Rev. Geophys.* **47**, RG1002 (2009).
43. J. Dunmore, J. Karlsson, *Independent Evaluation of FAO's Role and Work in Statistics* (Food and Agriculture Organisation, 2008).
44. K. Xiao, B. Womack, Distortion and credibility within China's internal information system. *J. Contemp. China* **23**, 680–697 (2014).

Acknowledgments: We would like to thank U. Wood-Sichra and K. Sonder for assistance with the Mexican crop statistics and Y. Kushnir for discussions about analyzing patterns of covariance. **Funding:** This project was supported by ACToday, a Columbia World Project. W.B.A. acknowledges funding from NSF-GRF DGE-11-44155; M.C., from NSF OCE 1657209; R.S., from NSF 1602581; and L.Y., from the Fundamental Research Funds for the Central Universities (program no. 2662018PY101). **Author contributions:** W.B.A., W.B., and L.Y. collected data for the analysis. W.B.A. performed the analysis. W.B.A., R.S., M.C., and W.B. analyzed the results. W.B.A., R.S., M.C., W.B., and L.Y. contributed to writing the paper. W.B.A., R.S., M.C., and W.B. contributed to the design of the study. **Competing interests:** The authors declare that they have no competing interests. **Data and materials availability:** All data needed to evaluate the conclusions in the paper are present in the paper and/or the Supplementary Materials. Additional data related to this paper may be requested from the authors.

Submitted 27 November 2018
Accepted 24 May 2019
Published 3 July 2019
10.1126/sciadv.aaw1976

Citation: W. B. Anderson, R. Seager, W. Baethgen, M. Cane, L. You, Synchronous crop failures and climate-forced production variability. *Sci. Adv.* **5**, eaaw1976 (2019).

ScienceAdvances

Synchronous crop failures and climate-forced production variability

W. B. Anderson, R. Seager, W. Baethgen, M. Cane and L. You

Sci Adv **5** (7), eaaw1976.
DOI: 10.1126/sciadv.aaw1976